Progress In Electromagnetics Research M, Vol. 107, 105–118, 2022

A Six-Port Slot Antenna System with Wideband and High-Isolation for 5G NR Bands

Weidong Mu[1], Zhonggen Wang[1, *], Ming Yang[2], Wenyan Nie[3], and Pan Wang[1]

Abstract—In this article, a slot-antenna array with wideband and high-isolation for multiple-input multiple-output (MIMO) systems is presented that can be used in fifth-generation new radio (5G NR) communication. The MIMO antenna system is realized by loading six identical antennas (Ant 1–Ant 6) into an FR4 substrate to form a six-port array for a 6×6 MIMO system. Each antenna element is a slot antenna type that is composed of a T-shaped open slot and an L-shaped $50\,\Omega$ microstrip line. Each T-shaped slot is formed by inserting an I-shaped open branch in the center of the ground plane's U-shaped slot. The L-shaped microstrip line is placed on the upper surface of FR4 to enable coupling feeding in the 3.3 to 5.10 GHz frequency range to cover the 5G NR bands N77/N78/N79. The isolation is increased to more than 18.1 dB by etching the T-shaped slot between the radiation elements on the metal plate. The proposed antenna system was fabricated and tested. The experimental results indicate that the MIMO system can cover the frequency range of 3.20–5.15 GHz with a return loss of 6 dB and provides isolation greater than 16.2 dB. Additionally, a total efficiency greater than 50% and envelope correlation coefficient of less than 0.02 are obtained. The performance under hand-on scenarios is also good. Simulated and measured results indicate that the stated results are consistent. The test results indicate that the antenna satisfies the 5G communication requirements.

1. INTRODUCTION

With faster data transmission and lower delay rates, fifth-generation communication (5G) increasingly meets user requirements for mobile communications compared to fourth-generation communications (4G). According to protocol specifications, 5G's data transmission rate can reach 100 times that of 4G. MIMO technology is becoming the key technology increasingly for multi-antenna operation due to its ability to provide massive data flow for the network and improve channel capacity effectively. There are many 5G communication technologies available. Still, the fifth-generation new radio (5G NR) communication system is introduced due to its channel capacity, transmission rate, and delay rate advantages. According to the 3G partnership project's technical specification 38.101, 5G NR is divided into two frequency bands. One is used for frequencies below 6 GHz, while the other is used for millimeter-wave frequencies [1]. It is widely accepted that bands below 3 GHz have been used in 3G/4G systems for a long period of time. WLAN-5 GHz operates at frequencies between 5 and 6 GHz (5.15–5.825 GHz). The 5G NR bands operating at frequencies N77 (3.3–4.2 GHz), N78 (3.3–3.8 GHz), and N79 (4.4–5 GHz) are expected to be widely adopted in communication networks due to their benefits for 5G networks.

In recent years, numerous studies have been conducted on MIMO antennas used in the 5G NR operation band [2–20]. Amid these studies, various antenna design techniques, such as inverted-F,

Received 20 November 2021, Accepted 6 January 2022, Scheduled 11 January 2022

* Corresponding author: Zhonggen Wang (zgwang@ahu.edu.cn).

[1] School of Electrical and Information Engineering, Anhui University of Science and Technology, Huainan 232001, Anhui, China. [2] Department of Electronics and Information Engineering, Bozhou University, Bozhou 236800, Anhui, China. [3] School of Mechanical and Electrical Engineering, Huainan Normal University, Huainan 232001, China.

planar inverted-F antenna (PIFA), monopole, and loop, have been proposed. To the above-mentioned structure, slot antennas have also been applied in 5G communication due to their simple structure, wide operation band, and easy integration of active equipment [21–27]. However, when being used for 5G NR band applications, these slot antennas still have significant margins for improvement in terms of bandwidth utilization and other areas.

Besides, the coupling between antenna elements is a major issue affecting the performance of MIMO systems. Various decoupling mechanisms have been presented in the literature to solve this issue, such as orthogonal polarization [28], defected ground structures [29, 30], and neutralization lines [31]. Self-isolation techniques [32–34] have also been investigated to further enhance the isolation. These decoupling techniques provide the foundation for improving the isolation of MIMO systems.

In this paper, we propose a six-port slot antenna for 5G NR with wide band and high isolation. Here, the method of metal plate slotting is used. An open branch is added in the middle of the original U-shaped slot to improve the impedance matching characteristics and create a T-shaped slot antenna. A coupling feeding scheme is adopted as an L-shaped branch that covers the 5G NR bands. Meanwhile, to improve element isolation, T-shaped slots are etched between successive antenna elements along an FR4 substrate to block the current transmission between the ports on the metal plate effectively. The optimized slot antenna has a bandwidth of 3.3 GHz to 5.10 GHz and an envelope correlation coefficient (ECC) of less than 0.02.

This article is organized as follows. In Section 2, the design process and operating mechanism of the MIMO system are discussed, including the designed structure, parameter analysis, and operating principle. In Section 3, the antenna fabrication and simulated and measured performances of the proposed MIMO system are presented. In Section 4, the performance under hand-held scenarios, including the single handset mode (SHM) and double handset mode (DHM), is discussed. In Section 5, a comparison chart is shown to highlight the advantages of the proposed design scheme. Finally, in Section 6 the conclusion of this article is drawn.

2. PROPOSED MIMO ANTENNA SYSTEM

2.1. Antenna Geometry

The overall structure of the proposed six-port slot antenna system is illustrated in Fig. 1(a), and the specific structure and size of the proposed antenna element are also shown in Fig. 1(b).

In Fig. 1(a), six antenna elements are placed along two sides of the FR4 substrate sprayed with tin on both sides ($\varepsilon_r = 4.4$, $\tan\delta = 0.02$). The size of the dielectric substrate is 150 mm × 75 mm × 0.8 mm,

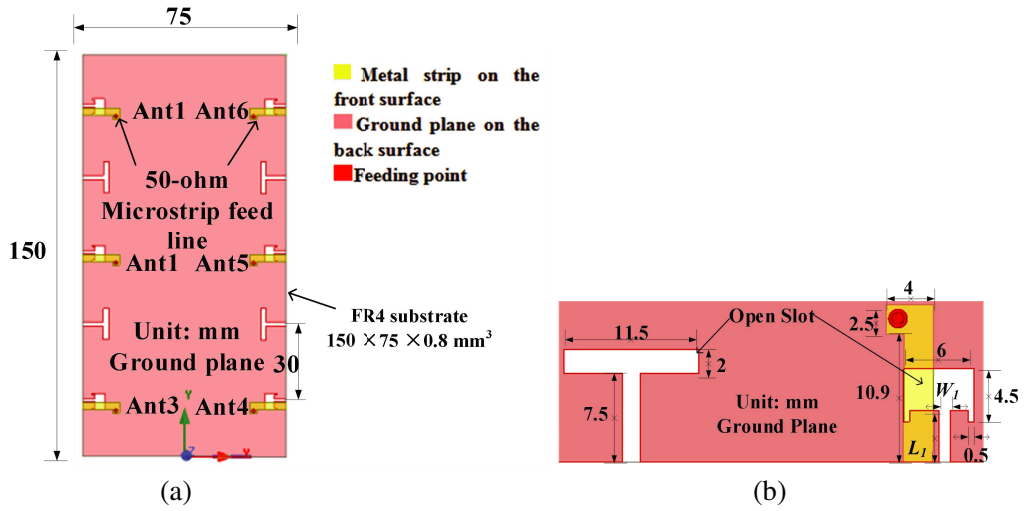

Figure 1. Geometry and dimensions of the proposed MIMO antenna system. (a) Perspective view. (b) Detailed structure of the slot antenna element (Ant 1).

making it suitable for 5.9-inch smartphones. Fig. 1(b) illustrates the antenna element's detailed structure (taking Ant 1 for example). Unlike traditional closed slot antennas, this one features an etched T-shaped slot radiator with an open branch. The slots, in this case, are divided into three sections: vertical slot, horizontal slot, and open branch slot. The length and width of the two vertical slots are 1 mm and 0.5 mm, respectively, while the length and width of the horizontal slot connected with the two vertical slots are 6 mm and 3.5 mm, respectively. A combination of I-shaped open branch and horizontal slots is etched on this basis. The size of the open branch is 4.4 mm × 1 mm. This extended open branch serves to increase the slot antenna's capacitance and introduce resonance points. At the feeding point, the slot resonator is coupled and fed via an L-shaped microstrip. It has horizontal and vertical dimensions of 4 mm and 10.9 mm, respectively, and a width of 2.5 mm.

2.2. Design and Corresponding Analysis

A U-shaped slot is a common antenna structure. Unlike most other U-shaped slots, which are narrow and long, the proposed U-shaped slot's width accounts for approximately 75% of its length. An open-branch is extended into it on this basis. To illustrate the open-branch's effect on the antenna element's performance, in Fig. 2(a) the antenna element without an etched I-shaped open-branch is compared to the proposed antenna element. Simultaneously, the element is used as a reference antenna element without etching the I-shaped slot. However, when these two antenna elements are placed in the upper left corner (the same location as Ant 1), the antenna element's performance is significantly different. As illustrated in Fig. 2(b), the reference antenna element's impedance matching performance is extremely poor. By contrast, the proposed antenna element generates 3.9 GHz and 4.3 GHz resonance modes by incorporating an I-shaped open branch in the middle of the U-shaped slot, which exhibits superior impedance matching characteristics.

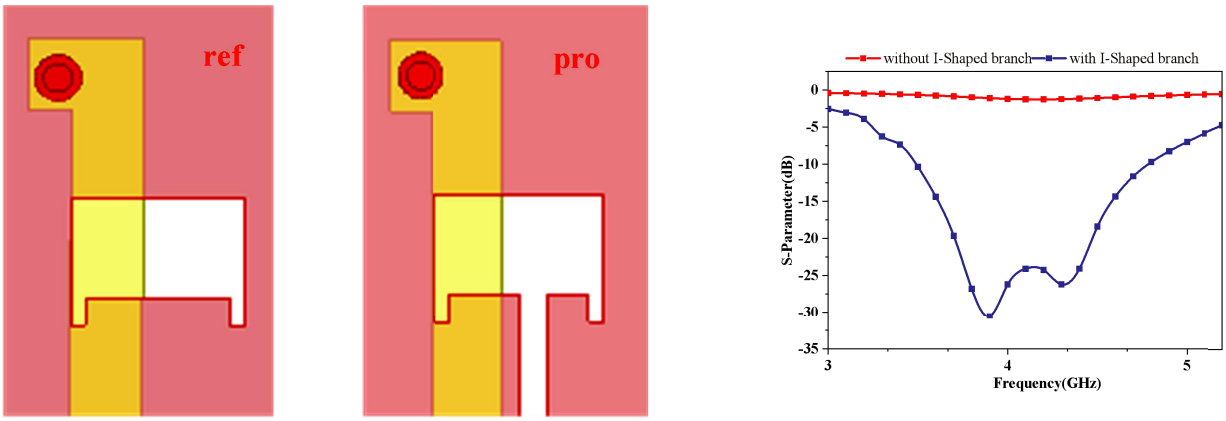

Figure 2. Evolution process of antenna element structure. (a) Reference and proposed. (b) Reflection coefficient of reference and proposed.

The length L_1 and width W_1 of the open-branch are critical parameters for impedance matching. Fig. 3 illustrates the simulated reflection coefficients for tuning L_1 and W_1. As illustrated in Fig. 3(a), the reflection coefficients are extremely low when the open-branch is not connected to the U-shaped slot ($L_1 < 4.4$ mm). It can exhibit exceptional impedance matching performance when being used in conjunction with other components (4.4 mm $< L_1 <$ 7.4 mm). As illustrated in Fig. 3(b), the impedance matching performance changes as W_1 varies. While broadband coverage is possible with a W_1 of 0.5 mm, the return loss is typically around 10 dB. When $W_1 = 1$ mm, the coverage of the N77/N78/N79 band can be realized with better impedance matching performance than that when $W_1 = 1.5$ mm.

To facilitate the intuitive analysis of the proposed antenna element's resonant mode and using Ant 1 as an example, Fig. 4 shows the current distribution diagram of the slot antenna element at

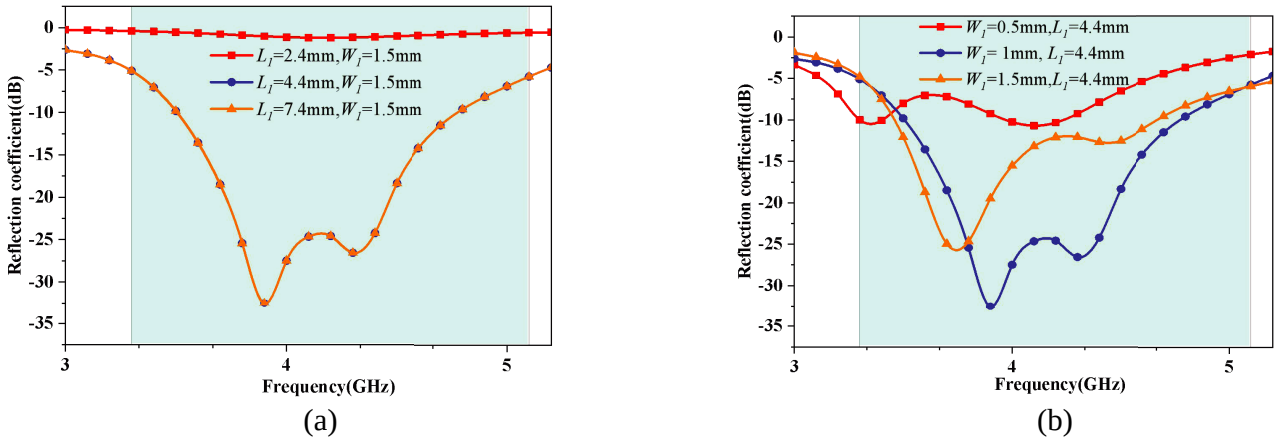

Figure 3. Simulated reflection coefficients of tuning (a) L_1, (b) W_1.

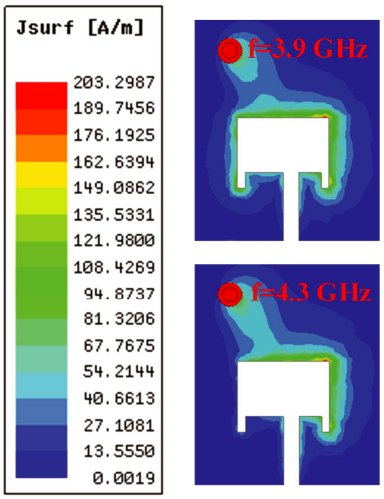

Figure 4. Current distribution of ground plane at resonant modes.

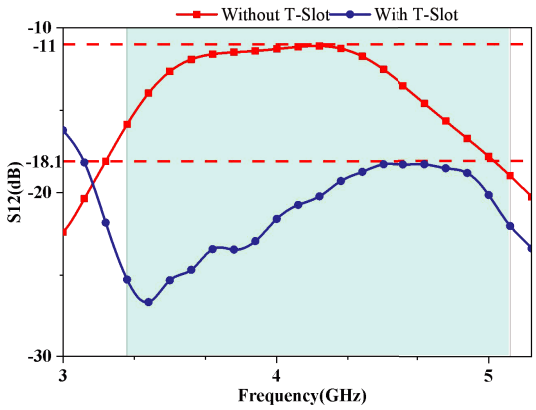

Figure 5. S_{12} parameters without and with T-shaped isolation slot.

3.9 GHz and 4.3 GHz. The current distribution diagram demonstrates that when the slot antenna operates at 3.9 GHz, the strong current is distributed primarily along the upper half and both sides of the T-shaped slot. The open-branch current is weak, and the current distribution does not have a zero point. The electric length of the strong current is 18 mm, which is approximately half the wavelength of the corresponding 3.9 GHz signal, indicating that the antenna operates in half-wavelength resonant mode at that frequency. When the slot antenna operates at 4.3 GHz, the strong current is concentrated on the half side of the T-shaped slot, with a length of 8.5 mm, which is roughly one-quarter of the corresponding wavelength of 4.3 GHz. This indicates that the antenna operates at 0.25λ resonant mode at 4.3 GHz (λ corresponding to 4.3 GHz wavelength). However, the weak current is still distributed around the T-shaped open-branch. The addition of I-shaped branches increases the capacitance of the slot antenna and significantly improves the antenna element's impedance matching characteristics.

T-shaped structures have been applied in different functions in electromagnetics, such as that demonstrated in [35], and T-shaped metamaterial absorbers exhibit excellent absorption performance. However, in this case, the T-shaped structure acts as an isolator. The coupling between the elements is primarily due to the metal plate's current transmission. To reduce the degree of coupling between antenna elements, a T-shaped slot is etched into the surface of the printed metal plate, effectively

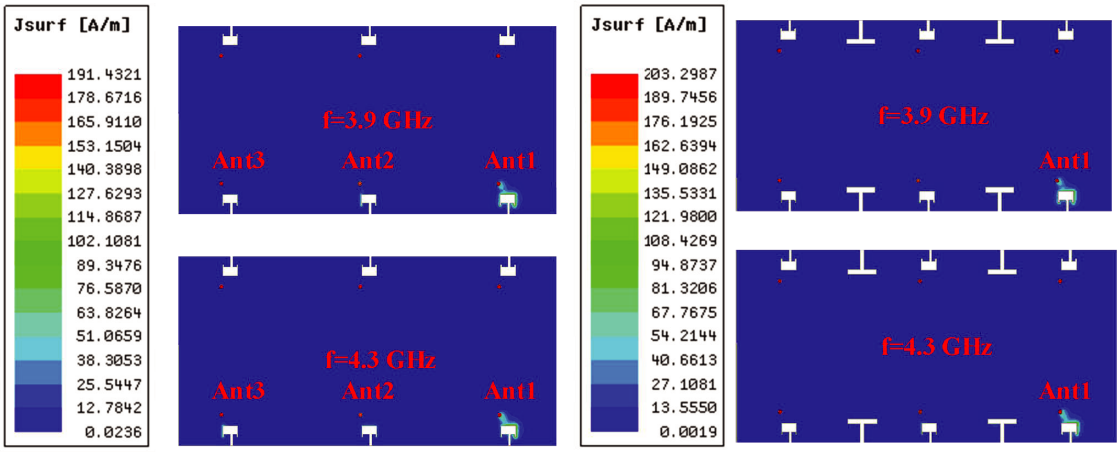

Figure 6. Current distribution of ground plane when Ant 1 is excited. (a) Without T-shaped slot. (b) With T-shaped slot.

blocking the current transmission across the metal plate's surface. Fig. 5 shows the transmission coefficients of the MIMO system without and with the proposed T-slots (taking S_{12} for example). As can be seen from Fig. 5, the isolation between the antenna ports has been greatly improved with the addition of the T-slots and reaches 18.1 dB or more. To demonstrate the effect of a T-shaped slot on coupling, Figs. 6(a) and (b) depict the current distribution of metal plates when Ant1 is excited alone. As illustrated in the figure, due to the existence of the T-shaped isolators, when Ant 1 is excited alone, less ground current diffuses to other ports, implying that a good isolation effect between ports is achieved.

3. RESULTS AND DISCUSSION

The proposed antenna array was fabricated, and its front and back views are shown in Fig. 7. The proposed six-port MIMO antenna system was simulated using ANSYS software, and its S-parameters

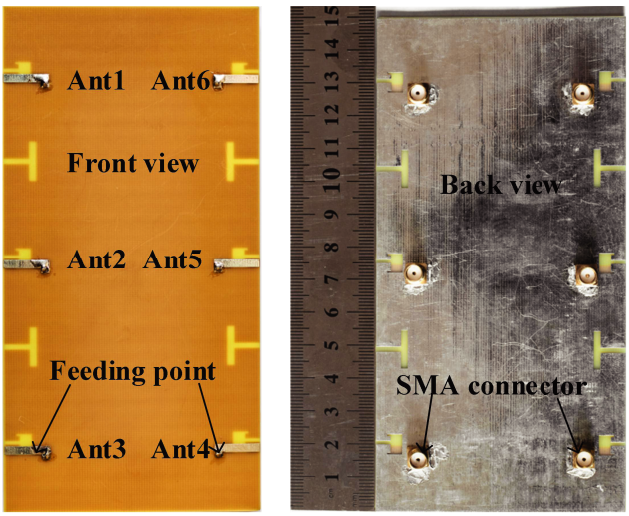

Figure 7. Fabricated prototype. (a) Front view. (b) Back view.

were determined using a Vector Network Analyzer. The far-field test was conducted in an anechoic microwave chamber. The corresponding results are presented and discussed in the following sections.

3.1. *S*-Parameters

Due to the symmetrical distribution of slot antennas, the simulated and measured *S*-parameter values are given here for only one side. As illustrated in Fig. 8(a), there were differences in the results of the reflection coefficients between simulation and measurement. The measured resonant frequency points deviate from the simulated values. The low-frequency resonance point, in particular, moved to the left. Compared to the simulated results, the high-frequency resonance point moved to the right, and the impedance matching performance improved. These differences may be the result of the manufacturing process or measurement errors. However, as illustrated in Fig. 8(a), the measured impedance bandwidth defined by the 6 dB return loss for Ant 1–3 was 3.20–5.15 GHz, which is sufficient to cover the desired band (3.3–5.1 GHz). In terms of transmission coefficients, as illustrated in Figs. 8(b) and (c), the differences between simulated and measured values were less noticeable and mainly related to measurement accuracy. The measured results indicate that the isolation between adjacent ports is greater than 16.2 dB, implying that the ports perform well with multiplexing and comply with the MIMO antenna communication standard.

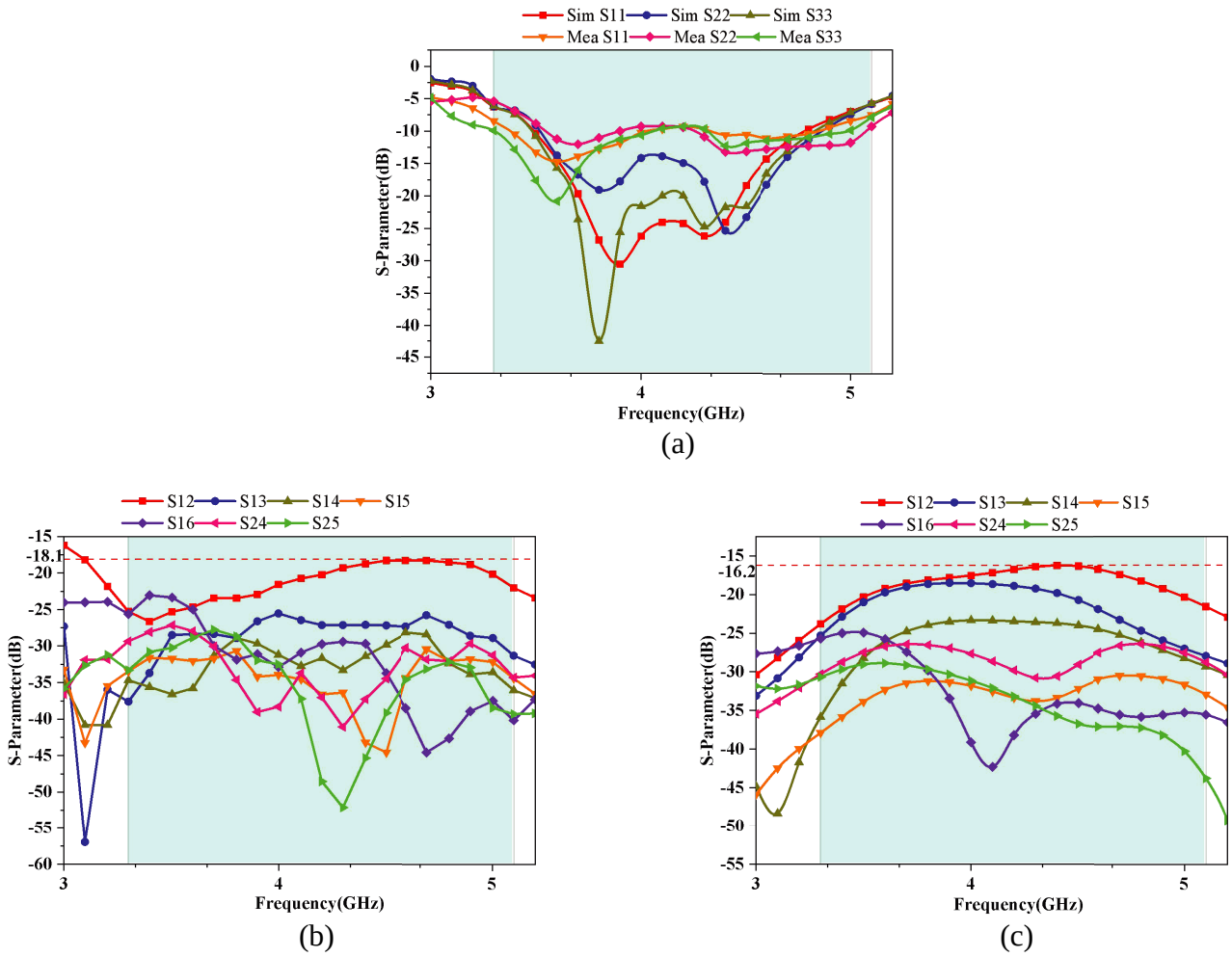

Figure 8. *S*-parameters. (a) Simulated and measured reflection coefficients. (b) Simulated transmission coefficients. (c) Measured transmission coefficients.

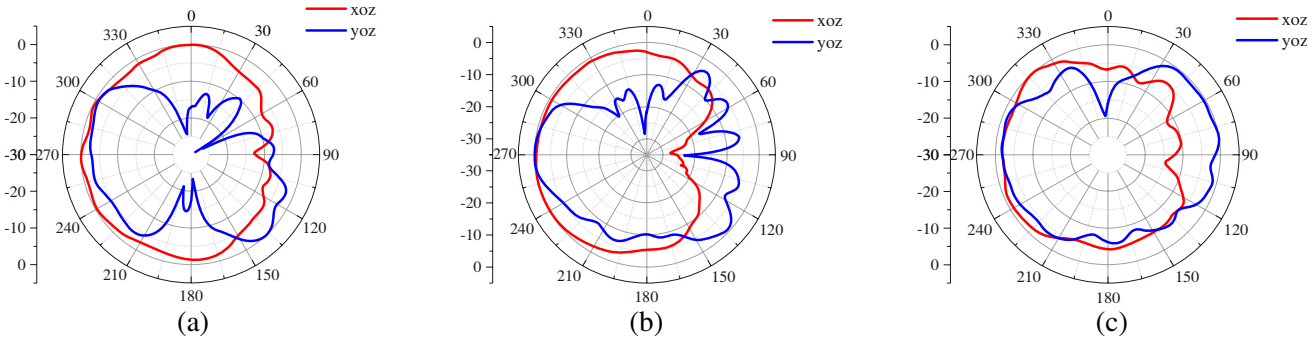

Figure 9. Measured radiation patterns for (a) Ant 1, (b) Ant 2, (c) Ant 3 at 3.9 GHz.

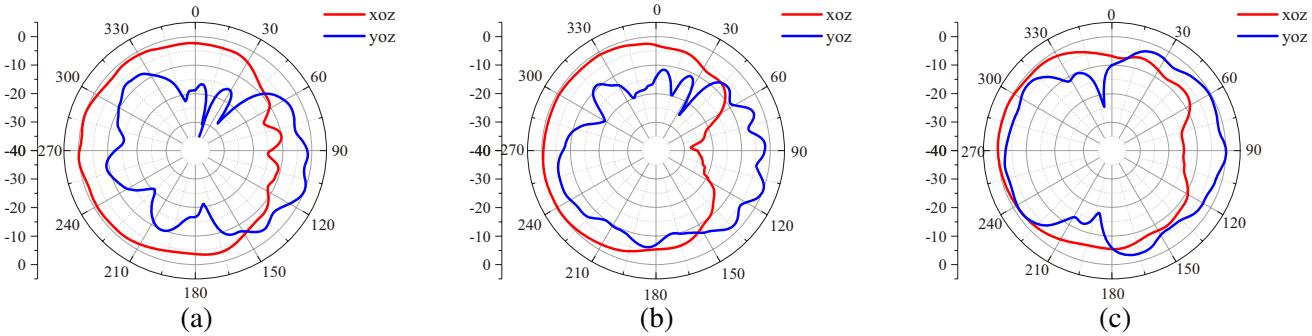

Figure 10. Measured radiation patterns for (a) Ant 1, (b) Ant 2, (c) Ant 3 at 4.3 GHz.

3.2. Radiation Performance

For mobile terminals, the radiation pattern around its direction should be good. Figs. 9 and 10 illustrate the test patterns for the XOZ and YOZ planes of Ant 1–3 in resonant modes. As can be seen, when the XOZ plane is used as the radiation plane, Ant 1–3's higher radiation gain directions are near 0°, 180°, and 270°. Ant 1–3, on the other hand, can produce omnidirectional radiation in the YOZ radiation plane effectively. Due to the mirror image distribution of the antenna elements, the antenna radiation directions are complementary, resulting in excellent far field radiation characteristics.

To provide a physical insight of the far field radiation performance of the proposed antenna element, Fig. 11 exhibits the simulated 3D radiation patterns. It is evident that the radiation pattern simulated using various resonance modes is slightly different when the port is the same. As shown in Fig. 11, when being fed through port 1 alone, the pattern has a radiation maximum along the $-x$ and $\pm z$ axes and a radiation minimum along approximately the $-y$ axis. However, the radiation maximum of port 3 in solo operation is around the $+x$ and $\pm z$ axes, and the radiation minimum is opposite to that of port 1 (along the $+y$ axis). From Figs. 11(c) and (d), it is evident that when being fed through port 2 alone, the pattern is different from those of port 1 or port 3. The pattern has a radiation maximum along the $-x$ axis and a radiation minimum along the y axis. Thus, good radiation pattern diversity is achieved at 3.9 GHz and 4.3 GHz, contributing to a high isolation response. The maximum gain in each mode can reach around 5 dB, fulfilling the requirement of high radiation gain.

Figure 12 illustrates the simulated and measured total efficiencies. Clearly, the measured total efficiencies are between 50% and 63% in the operation bandwidth, which was approximately 13% lower than the simulated values. Nevertheless, all measured total efficiencies were greater than 50%, indicating that high antenna efficiency was achieved.

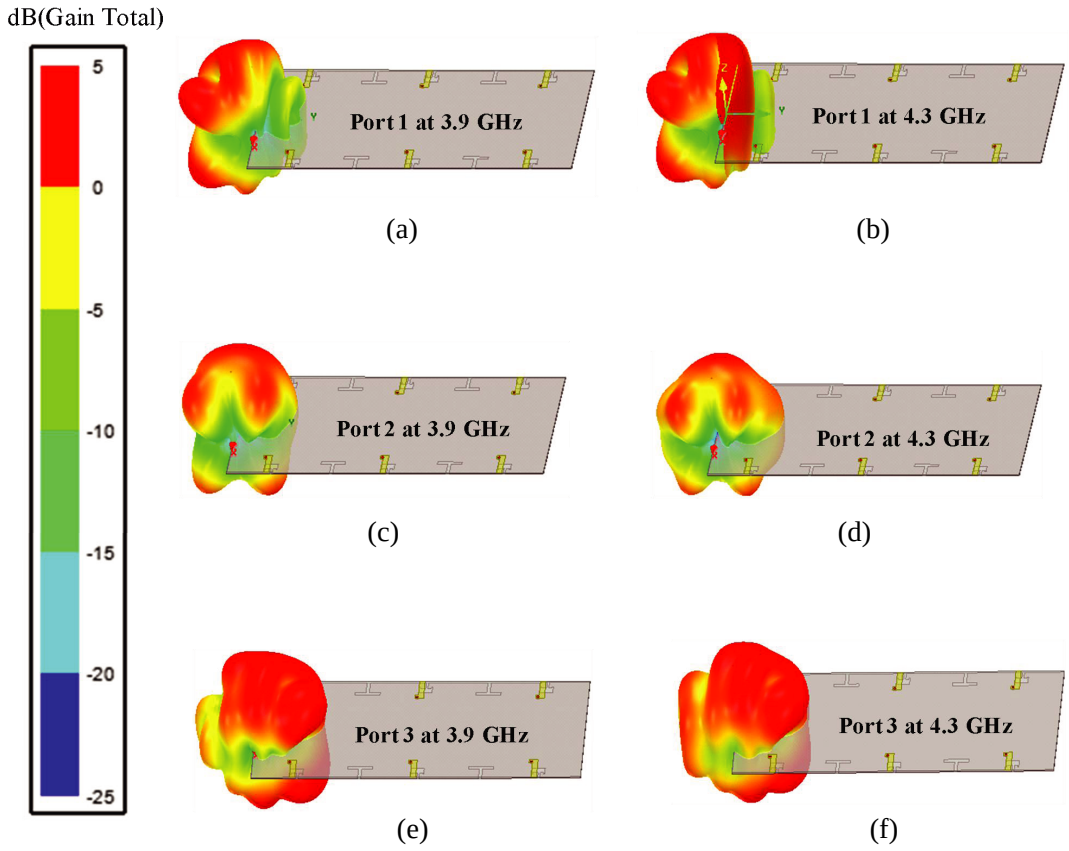

Figure 11. Simulated 3D radiation pattern. (a) Port 1 excited at 3.9 GHz. (b) Port 1 excited at 4.3 GHz. (c) Port 2 excited at 3.9 GHz. (d) Port 2 excited at 4.3 GHz. (e) Port 3 excited at 3.9 GHz. (f) Port 3 excited at 4.3 GHz.

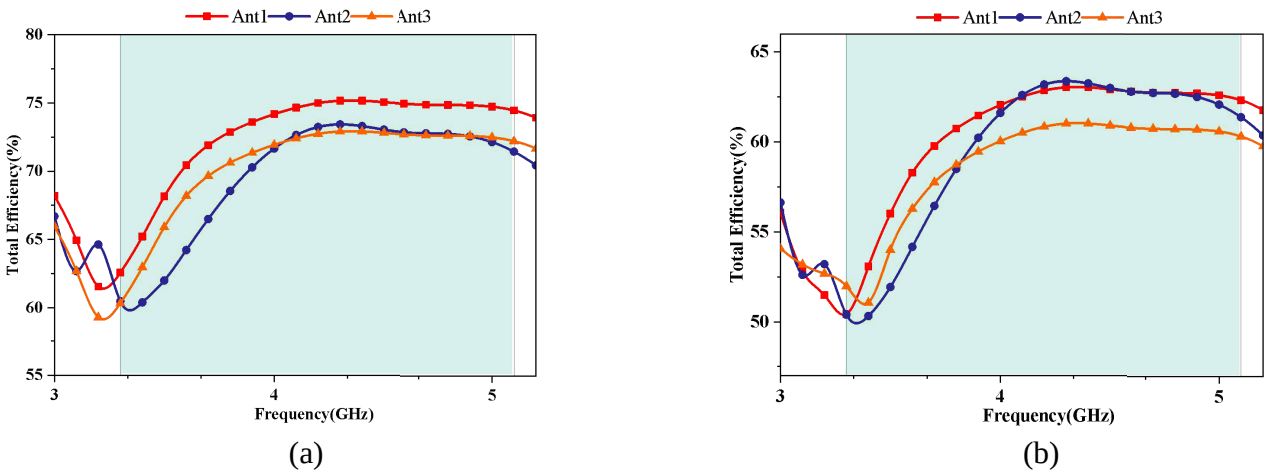

Figure 12. Total efficiency. (a) Simulated. (b) Measured.

3.3. Multiplexing Performance

Envelope correlation coefficient (ECC) is a critical metric for determining the radiation pattern diversity performance of MIMO antennas. The value of ECC reflects the quality of the correlation between the antennas. Lower ECC values correspond to lower degrees of mutual coupling between the antennas and smaller influence of each antenna on the other when they operate independently, representing an excellent MIMO system function. The ECC of a MIMO antenna used in modern mobile terminals must be less than 0.5 [24]. The equation for the calculation is as follows [36]:

$$\mathrm{ECC} = \frac{\left|S_{ii} * S_{ij} + S_{ji} * S_{jj}\right|^2}{\left(1 - \left|S_{ii}\right|^2 - \left|S_{ji}\right|^2 \left(1 - \left|S_{jj}\right|^2 - \left|S_{ji}\right|^2\right)\right)} \tag{1}$$

As illustrated in Fig. 13, the ECC values were less than 0.02. Across the operation bandwidth, the largest ECC (between Ant 1 and Ant 2) was only 0.019, indicating an acceptable level of diversity performance.

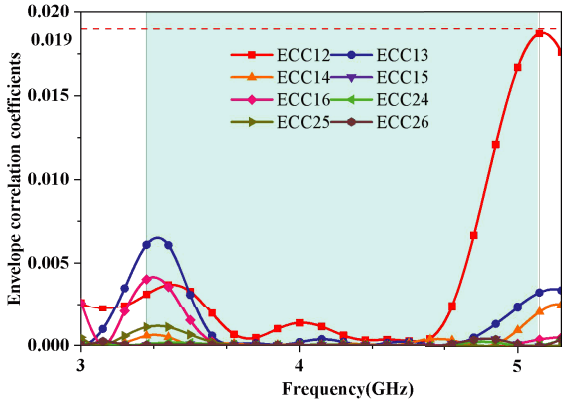

Figure 13. Calculated ECCs.

4. PRACTICAL APPLICATION ANALYSIS

In this section, the effect of practical antenna performance is discussed. The most frequently used operation modes are single handset mode (SHM) and double handset mode (DHM). Fig. 14 depicts the simulated application scenario. The effect on the user's head will not be discussed here, as the operation is used exclusively for data transmission, not for call mode.

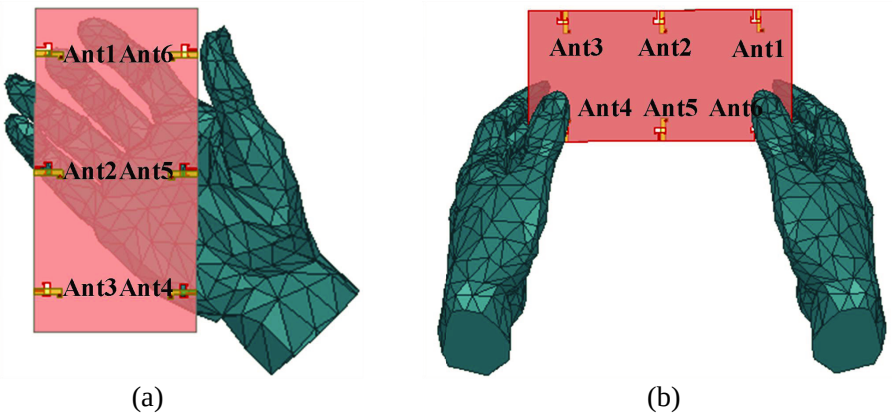

Figure 14. Two application scenarios of hand-held smartphone. (a) SHM. (b) DHM.

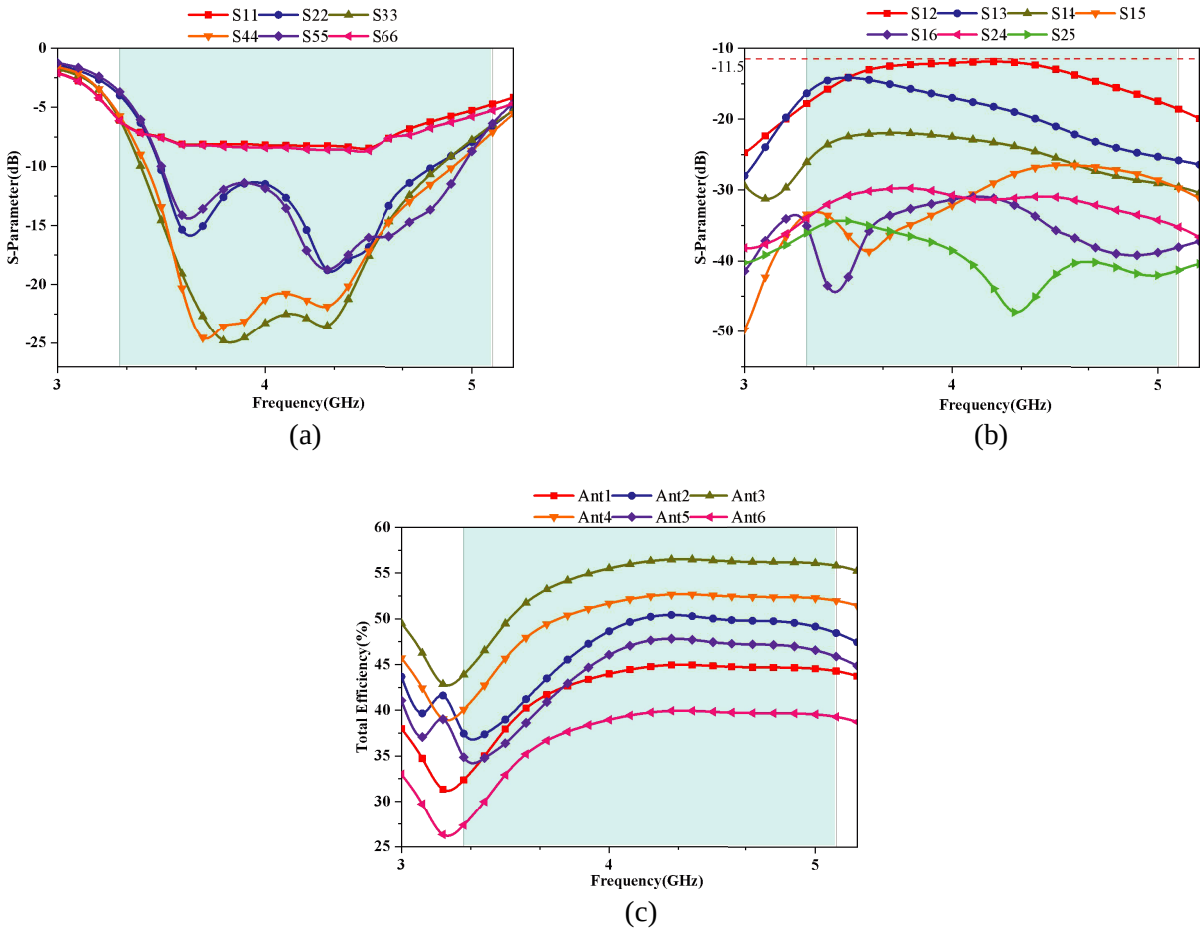

Figure 15. Simulated parameters under SHM. (a) Reflection coefficient. (b) Transmission coefficient. (c) Total efficiency.

As illustrated in Fig. 14(a), Ant 1 and Ant 6 exhibit high reflection coefficients for SHM due to their direct contact with fingers. In comparison, Ant 2, 3, 4, and 5's reflection coefficients were slightly less affected because they were further away from the fingers and still covered the 3.3–5.1 GHz band. However, the reflection coefficients remain slightly higher than in the absence of hand interference. Despite this, isolation can be greater than 11.5 dB across the entire operating frequency band. As illustrated in Fig. 15(c), because hand tissue can absorb electromagnetic waves, Ant 1 and Ant 6 radiation efficiencies were reduced to less than 40%. Due to the close proximity to the palm, the efficiencies of Ant 2 and Ant 5 were also reduced by about 18%. In comparison, Ant 3 and Ant 4 were located far from the hand and exhibited greater than 55% efficiency.

For DHM, only Ant 4 and Ant 6 were in direct contact with fingers, as illustrated in Fig. 14(b). All other antenna elements were not in direct contact with fingers. Because Ant 4 and Ant 6 were covered by the thumbs, their reflection coefficients were significantly increased. The resonant points shifted to the right, resulting in significantly worse impedance matching. While their resonant frequencies were not significantly different from those of other antenna elements, their impedance matching was also worse than that in the absence of interference. However, between ports, a good isolation performance of more than 11 dB was still maintained. As illustrated in Fig. 16(c), the radiation efficiencies of these antenna elements that were not in contact with fingers or palms remained greater than 50% throughout the operating bandwidth. In comparison, when Ant 4 and Ant 6 were in contact with fingers, their efficiency was significantly reduced, and the maximum efficiency was only around 45%.

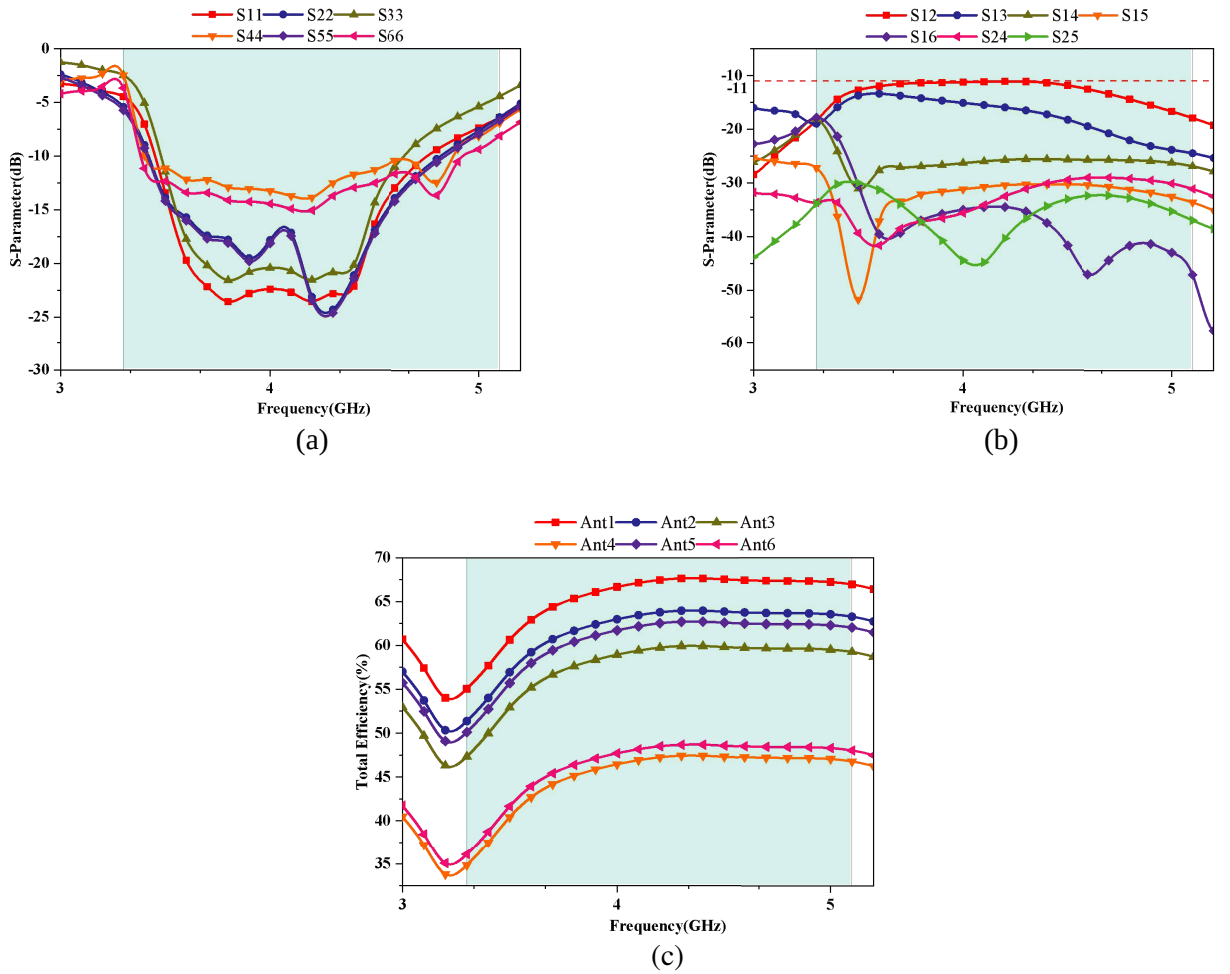

Figure 16. Simulated parameters under DHM. (a) Reflection coefficient. (b) Transmission coefficient. (c) Total efficiency.

Table 1. Performance comparison of 5G antenna array.

References	Bandwidth (GHz)	Isolation (dB)	ECC	Total Efficiency (%)
Pro.	3.2–5.15 (−6 dB)	> 16.2	< 0.02	50–63
[3]	3.4–3.6 (−10 dB)	> 10	< 0.2	62–78
[5]	3.4–3.6 (−6 dB)	> 12.7	< 0.13	35–64
[9]	3.4–3.625, 3.90–4.55 (−10 dB)	> 20.1	< 0.3	> 40
[10]	3.3–3.6 (−6 dB)	> 15	< 0.15	45–60
[14]	3.4–3.6 (−6 dB)	> 10	> 0.15	40–52
[15]	3.4–3.6 (−6 dB)	> 14	< 0.15	40–52
[18]	3.4–3.6, 4.8–5.1 (−6 dB)	> 11.5	< 0.08	40–85
[21]	3.3–4.2 (−6 dB)	> 9.5	< 0.06	40–58
[22]	3.4–3.6 (−6 dB)	> 11	< 0.23	40–53
[24]	3.3–3.9 (−6 dB)	> 15	< 0.01	> 60
[27]	3.4–3.6 (−10 dB, 5G modules)	> 12	< 0.02	60–90
[28]	3.39–3.67 (−10 dB)	> 17.5	< 0.036	62–76

5. COMPARISON AND DISCUSSION

To illustrate the proposed antenna array's advantages, Table 1 compares the proposed work to several designs presented previously. As shown in Table 1, the proposed antenna array has a wider bandwidth than those of previous works. Additionally, the proposed design achieves a higher degree of isolation. The bandwidth constraint is overcome at a lower cost in terms of overall efficiency. Since it achieves high isolation and spatial reuse, it is an excellent candidate for 5G NR communication.

6. CONCLUSION

This paper proposed a six-port wideband and high-isolation antenna array for the 5G NR operation band of mobile terminals. Broadband is achieved in this case by loading an I-shaped open branch onto the slot antenna element's metal plate. Meanwhile, good isolation is achieved by etching a T-shaped slot along the substrate between the antenna elements. The proposed antenna array successfully covers the desired band (3.20–5.15 GHz), which corresponds to the N77/N78/N79 band of 5G. The critical performance indices are excellent, including suppressed mutual coupling (< -16.2 dB), acceptable antenna total efficiency (50%–63%), excellent envelope correlation coefficient (< 0.02), and excellent far-field radiation patterns. Additionally, this work simulated the practical application of the proposed antenna array in data transmission mode. The corresponding results demonstrate that the proposed antenna array still performs well in this scenario.

ACKNOWLEDGMENT

This work was supported in part by the Natural Science Foundation of Anhui Provincial Education Department under Grant No. KJ2020A0307, and No. KJ2020A0768, in part by the Anhui Provincial Natural Science Foundation of China under Grant 2108085MF200 and 1808085MF166, in part by the Academic Funding Project for Distinguished Top Talents of Colleges and Universities in Anhui Province under Grant No. gxbjZD2021088, and in part by Graduate Innovation Fund of Anhui University of Science and Technology under Grant No. 2021CX2070.

REFERENCES

1. Chen, H.-D., Y.-C. Tsai, C.-Y.-D. Sim, and C. Kuo, "Broadband eight-antenna array design for sub-6 GHz 5G NR bands metal-frame smartphone applications," *IEEE Antennas and Wireless Propagation Letters*, Vol. 19, No. 7, 1078–1082, 2020.
2. Bait-Suwailam, M. M., T. S. Almoneef, and S. M. Saeed, "Wideband MIMO antenna with compact decoupling structure for 5G wireless communication applications," *Progress In Electromagnetics Research Letters*, Vol. 100, 117–125, 2021.
3. Ban, Y.-L., C. Li, C.-Y.-D. Sim, G. Wu, and K.-L. Wong, "4G/5G multiple antennas for future multi-mode smartphone applications," *IEEE Access*, Vol. 4, 2981–2988, 2016.
4. Cai, Q., Y. Li, X. Zhang, and W. Shen, "Wideband MIMO antenna array covering 3.3–7.1 GHz for 5G metal-rimmed smartphone applications," *IEEE Access*, Vol. 7, 142070–142084, 2019.
5. Chang, L., Y. Yu, K. Wei, and H. Wang, "Polarization-orthogonal co-frequency dual antenna pair suitable for 5G MIMO smartphone with metallic bezels," *IEEE Transactions on Antennas and Propagation*, Vol. 67, No. 8, 5212–5220, 2019.
6. Hu, W., et al., "Dual-band ten-element MIMO array based on dual-mode IFAs for 5G terminal applications," *IEEE Access*, Vol. 7, 178476–178485, 2019.
7. Jaglan, N., S. D. Gupta, B. K. Kanaujia, and M. S. Sharawi, "10 element sub-6-GHz multi-band double-T based MIMO antenna system for 5G smartphones," *IEEE Access*, Vol. 9, 118662–118672, 2021.
8. Jain, P., A. Thourwa, N. Sardana, S. Kumar, N. Gupta, and A. K. Singh, "I-shaped metamaterial antenna for X-band applications," *2017 Progress In Electromagnetics Research Symposium — Spring (PIERS)*, 2800–2803, St Petersburg, Russia, May 22–25, 2017.

9. Jha, P., A. Kumar, A. De, and R. K. Jain, "Modified CSRR based dual-band four-element MIMO antenna for 5G smartphone communication," *Progress In Electromagnetics Research Letters*, Vol. 101, 35–42, 2021.
10. Jiang, W., B. Liu, Y. Cui, and W. Hu, "High-isolation eight-element MIMO array for 5G smartphone applications," *IEEE Access*, Vol. 7, 34104–34112, 2019.
11. Liu, D. Q., H. J. Luo, M. Zhang, H. L. Wen, B. Wang, and J. Wang, "An extremely low-profile wideband MIMO antenna for 5G smartphones," *IEEE Transactions on Antennas and Propagation*, Vol. 67, No. 9, 5772–5780, 2019.
12. Parchin, N. O., H. J. Basherlou, I. A. Yasir Al-Yasir, M. Sajedin, J. Rodriguez, and R. A. Abd-Alhameed, "Multi-mode smartphone antenna array for 5G massive MIMO applications," *2020 14th European Conference on Antennas and Propagation (EuCAP)*, 1–4, 2020.
13. Piao, H., Y. Jin, and L. Qu, "Isolated ground-radiation antenna with inherent decoupling effect and its applications in 5G MIMO antenna array," *IEEE Access*, Vol. 8, 139892–139902, 2020.
14. Srinivasarao, G., "Algorithm approach to multiple input multiple output (MIMO) systems," *Int. J. Innov. Res. Comput. Commun. Eng.*, Vol. 3, No. 2, 11918–11924, 2015.
15. Wong, K.-L., C.-Y. Tsai, and J.-Y. Lu, "Two asymmetrically mirrored gap-coupled loop antennas as a compact building block for eight-antenna MIMO array in the future smartphone," *IEEE Transactions on Antennas and Propagation*, Vol. 65, No. 4, 1765–1778, 2017.
16. Yuan, X.-T., Z. Chen, T. Gu, and T. Yuan, "A wideband PIFA-pair-based MIMO antenna for 5G smartphones," *IEEE Antennas and Wireless Propagation Letters*, Vol. 20, No. 3, 371–375, 2021.
17. Zhang, X., Y. Li, W. Wang, and W. Shen, "Ultra-wideband 8-port MIMO antenna array for 5G metal-frame smartphones," *IEEE Access*, Vol. 7, 72273–72282, 2019.
18. Zhao, A. and Z. Ren, "Size reduction of self-isolated MIMO antenna system for 5G mobile phone applications," *IEEE Antennas and Wireless Propagation Letters*, Vol. 18, No. 1, 152–156, 2019.
19. Zhao, A. and Z. Ren, "Wideband MIMO antenna systems based on coupled-loop antenna for 5G N77/N78/N79 applications in mobile terminals," *IEEE Access*, Vol. 7, 93761–93771, 2019.
20. Zhao, X., S. P. Yeo, and L. C. Ong, "Decoupling of inverted-F antennas with high-order modes of ground plane for 5G mobile MIMO platform," *IEEE Transactions on Antennas and Propagation*, Vol. 66, No. 9, 4485–4495, 2018.
21. Barani, I. R. R., K.-L. Wong, Y.-X. Zhang, and W.-Y. Li, "Low-profile wideband conjoined open-slot antennas fed by grounded coplanar waveguides for 4×4 5G MIMO operation," *IEEE Transactions on Antennas and Propagation*, Vol. 68, No. 4, 2646–2657, 2020.
22. Chen, S.-C., L.-C. Chou, C.-I. G. Hsu, and S.-M. Li, "Compact sub-6-GHz four-element MIMO slot antenna system for 5G tablet devices," *IEEE Access*, Vol. 8, 154652–154662, 2020.
23. Jaglan, N., S. D. Gupta, and M. S. Sharawi, "18 element massive MIMO/diversity 5G smartphones antenna design for sub-6 GHz LTE bands 42/43 applications," *IEEE Open Journal of Antennas and Propagation*, Vol. 2, 533–545, 2021.
24. Li, Y., C.-Y.-D. Sim, Y. Luo, and G. Yang, "High-isolation 3.5 GHz eight-antenna MIMO array using balanced open-slot antenna element for 5G smartphones," *IEEE Transactions on Antennas and Propagation*, Vol. 67, No. 6, 3820–3830, 2019.
25. Parchin, N. O., et al., "Eight-element dual-polarized MIMO slot antenna system for 5G smartphone applications," *IEEE Access*, Vol. 7, 15612–15622, 2019.
26. Ullah, R., S. Ullah, R. Ullah, F. Faisal, I. B. Mabrouk, and M. J. A. Hasan, "A 10-ports MIMO antenna system for 5G smart-phone applications," *IEEE Access*, Vol. 8, 218477–218488, 2020.
27. Yuan, X.-T., W. He, K.-D. Hong, C.-Z. Han, Z. Chen, and T. Yuan, "Ultra-wideband MIMO antenna system with high element-isolation for 5G smartphone application," *IEEE Access*, Vol. 8, 56281–56289, 2020.
28. Li, M., Z. Xu, Y. Ban, Q. Yang, and Q. Zhou, "Eight-port dual-polarized MIMO antenna for 5G smartphone applications," *2016 IEEE 5th Asia-Pacific Conference on Antennas and Propagation (APCAP)*, 195–196, 2016.

29. Deng, J., J. Li, L. Zhao, and L. Guo, "A dual-band inverted-F MIMO antenna with enhanced isolation for WLAN applications," *IEEE Antennas and Wireless Propagation Letters*, Vol. 16, 2270–2273, 2017.
30. Dong, J., X. Yu, and L. Deng, "A decoupled multiband dual-antenna system for WWAN/LTE smartphone applications," *IEEE Antennas and Wireless Propagation Letters*, Vol. 16, 1528–1532, 2017.
31. Wang, Y. and Z. Du, "A wideband printed dual-antenna with three neutralization lines for mobile terminals," *IEEE Transactions on Antennas and Propagation*, Vol. 62, No. 3, 1495–1500, 2014.
32. Fu, Z. and W. Shen, "Eight-element self-decoupled MIMO antenna design for 5G smartphones," *International Journal of RF and Microwave Computer-Aided Engineering*, Vol. 31, No. 3, Art no. e22523, 2021.
33. Wong, K., C. Wan, and L. Chen, "Self-decoupled compact metal-frame LTE MIMO antennas for the smartphone," *Microwave and Optical Technology Letters*, Vol. 60, No. 5, 1170–1179, 2018.
34. Zhao, A. and Z. Ren, "Multiple-input and multiple-output antenna system with self-isolated antenna element for fifth-generation mobile terminals," *Microwave and Optical Technology Letters*, Vol. 61, No. 1, 20–27, 2019.
35. Jain, P., et al., "Ultra-thin metamaterial perfect absorbers for single-/dual-/multi-band microwave applications," *IET Microwaves, Antennas and Propagation*, Vol. 14, No. 5, 448–455, 2020.
36. Sharawi, M. S., "Printed multi-band MIMO antenna systems and their performance metrics [wireless corner]," *IEEE Antennas and Propagation Magazine*, Vol. 55, No. 5, 218–232, 2013.